J Solid State Electrochem (2001) 5: 538–545
DOI 10.1007/s100080000180

ORIGINAL PAPER

**Mohamed Mohamedi · Yasunari Hisamitsu
Takashi Kudo · Takashi Itoh · Isamu Uchida**

Explicit study on the oxidation mechanism of nickel in molten Li_2CO_3-K_2CO_3

Received: 4 August 2000 / Accepted: 11 October 2000 / Published online: 24 May 2001

Abstract The oxidation behavior of nickel in Li + K carbonate melt is followed by measuring the open-circuit potential and by electrochemical impedance spectroscopy under an $O_2 + CO_2$ gas mixture in the ratio 90/10 at a total pressure of 1 atm at 650 °C. X-ray diffraction (XRD) and energy-dispersive spectroscopy are employed for qualitative and quantitative analyses of the different compounds involved during the oxidation of nickel. Atomic force microscopy is used for both imaging the evolution of the oxide layer and determining its surface roughness. The in situ oxidation process of nickel demonstrates three stages: rapid formation of a compact surface oxide (first stage), thicker oxide layer (second stage), and a porous oxide structure (third stage). The lithiation reaction has been identified to occur during the second stage. Formation of an intermediate and unstable compound, namely $NiCO_3$, has been confirmed by XRD.

Keywords Molten carbonates · Nickel oxidation · Lithiation · Impedance spectroscopy

Introduction

One of the major causes of molten carbonate fuel cells' (MCFCs) performance limitation is provoked by the fact that the NiO cathode is unsatisfactory for long-term operation owing to its considerable dissolution rate and tendency to cause cell shorting. Alternative cathode materials are being sought to replace NiO. The present study is part of a systematic investigation program focused on the possibilities of extending the lifetime of MCFCs to 40,000 h in order to render them commercially viable. As alternative cathode materials, nickel in nickel-based alloys and in iron-based alloys are being considered in our laboratory. Insights into the structure (porosity or roughness) and performance of the NiO cathode have yet to be established and remain a very important basic research necessity.

Nishina et al. [1] investigated the in situ formation of NiO in molten Li + K carbonate using open circuit potential (OCP) measurements. Three potential plateaus were observed which were ascribed to (1) oxidation of Ni to NiO, (2) oxidation of Ni(II) to Ni(III) involving a lithiation, and (3) an oxygen electrode reaction. Tomczyk et al. [2] suggested the existence of a Ni(II)/Ni(III) system in which the formation of Ni(III) could be related to the lithiation of the NiO electrode. Tomczyk et al. [3] have subsequently reconsidered that oxidation of Ni proceeds by decomposition of an unstable compound, which has yet to be clearly identified. Young Yang and Young Kim [4] using an OCP method have investigated the oxidation behavior of Ni in a molten Li + K carbonate eutectic. The in situ oxidation process of Ni showed the presence of three potential plateaus. The first and second plateaus were attributed to the nucleation and growth of the oxide, respectively. The final plateau was ascribed to an oxygen electrode reaction. The authors deduced that the lithiation takes place by chemical reaction at the growth step of the oxide. According to Yazici and Selman [5], the three stages correspond to the rapid formation of a compact surface oxide (first stage) → thicker oxide layer (second stage) → porous oxide structure (third stage).

The oxidation of nickel in molten carbonate reported in the works cited above [1, 2, 3, 4, 5] was examined by measuring the OCP versus time profile. To our best knowledge, very few works dealing with the oxidation of

M. Mohamedi (✉) · Y. Hisamitsu · T. Itoh · I. Uchida
Department of Applied Chemistry,
Graduate School of Engineering, Tohoku University,
07 Aramaki-Aoba, Aoba-Ku,
Sendai 980-8579, Japan
E-mail: mohamed@est.che.tohoku.ac.jp
Tel.: +81-22-2177218
Fax: +81-22-2148646

T. Kudo
Research and Development Center,
Tohoku Electric Power Co. Inc.,
7-2-1 Nakayama, Aoba-Ward,
Sendai 981-0952, Japan

nickel by impedance spectroscopy have been reported in the literature [6, 7]. The method has been applied to the nickel/molten Na_2CO_3 interface at 1000 °C and 1 atm CO_2 [6], and to the nickel/Li_2CO_3-K_2CO_3 (62–38 mol%) interface at 650 °C under reducing fuel gas atmospheres of 64%H_2-16%CO_2-20%H_2O [7].

In this work, we report new investigations of the oxidation of nickel in the molten Li_2CO_3-K_2CO_3 (62–38 mol%) eutectic under an oxidizing atmosphere of an O_2/CO_2 gas mixture in the ratio of 90/10 at a total pressure of 1 atm. Three separate procedures were adopted as follows:

1. The first step consisted in recording the OCP versus time of the nickel electrode in order to identify the different stages related to the oxidation of nickel and the lithiation step.
2. The different products involved during the different stages of the oxidation of the nickel electrode were characterized and quantified by analytical techniques such as X-ray diffractometry (XRD) and energy dispersive spectroscopy (EDS). The surface topography was observed by atomic force microscopy (AFM).
3. Finally, the mechanism of oxidation was monitored by recording impedance spectra obtained at different stages of the OCP versus time profile.

The objective is to shed further light on the formation mechanism of nickel oxide in molten carbonates. Results deduced from this work will help obtain insight into the influence of nickel on the corrosion behavior of nickel-based alloys.

Experimental

Melt purification, gas handling, and cell assembly have been described previously [8, 9, 10]. The working electrode consisted of a thin layer (ca. 0.75 μm) of Ni sputtered on a gold flag (0.39 cm^2), which was fully immersed in the melt. The counter electrode was a coiled gold wire (1 mm diameter, 15 cm length). All the potentials reported in this work were referred to the standard Au|($0.33O_2 + 0.67CO_2$) gas reference electrode denoted henceforth as SOE. Electrochemical measurements were carried out in a mixture of 62% lithium carbonate and 38% potassium carbonate. The cell temperature was kept at 923 ± 1 K and was monitored by an Alumel-Chromel thermocouple sheathed in a protective alumina tube. A gas cylinder of premixed $O_2/CO_2 = 90/10$ supplied by Sumitomo Seika Chemicals was used. The total pressure was fixed to 1 atm.

Prior to testing and after exposure the samples were examined by XRD (Shimadzu XD-D1 diffractometer using Cu Kα radiation). Surface morphologies were examined by AFM (Nanoscope IIIa Controller) using a silicon tip in tapping mode. Samples withdrawn from the melt were dipped into water, afterwards dried in the oven at 120 °C for one night, then submitted to XRD or AFM analysis.

The electrochemical impedance spectroscopy (EIS) studies generally covered a frequency range from 10 kHz to 1 or 0.1 Hz and were performed using Solartron's 1286 electrochemical interface and a 1260-frequency response analyzer. The spectra were recorded at the OCP, using a superimposed voltage signal of 5 mV amplitude. Fitting of the empirical data was performed using the non-linear least-squares minimization method called "EQUIVCRT" developed by Boukamp [11]. This program fits simultaneously the imaginary and the real parts of the impedance data and provides uncertainty estimates for all estimated parameters, thus obtaining the optimum fit to the measured dispersion data. We tried to find an acceptable fit that agreed with the proposed mechanism in the whole frequency range that we used. A fit was considered to be adequate when the value of χ^2 given by the program was of the order of 10^{-4} or less and the average estimated error, δ, in the error plots not greater than 3%.

The frequency response of the nickel specimen was postulated to be indicative of diffusion behavior that is affected by the surface topography. Accordingly, a constant phase element (CPE or Q) was used for equivalent circuits. The general expression for the admittance response of the CPE is [11]:

$$Y_Q = Y_0\omega^n \cos(n\pi/2) + jY_0\omega^n \sin(n\pi/2) \quad (1)$$

where ω is the angular frequency, which is $2\pi f$ with f being the frequency, and $j = (-1)^{1/2}$. The parameter n can be discussed in terms of diffusion phenomena, surface morphology, and dissipative processes. Depending on the n value, the CPE can have a variety of responses. If $n = 0$, it represents a resistance with $R = Y_0^{-1}$; if $n = 1$, it represents a capacitance with $C = Y_0$; and if $n = 0.5$, it represents a Warburg response. Note that with $n = 0.5$, Eq. 1 becomes:

$$Y_W = Y_0(j\omega)^{1/2} \quad (2)$$

which is the admittance response of the Warburg element that relates to Fick's second law for a semi-infinite diffusion process.

Results

OCP measurements

The OCP response of a fully immersed nickel electrode is presented in Fig. 1. Three distinct stages are observed for nickel oxidation in contact with molten carbonate. In stage I, the nickel electrode potential was initially

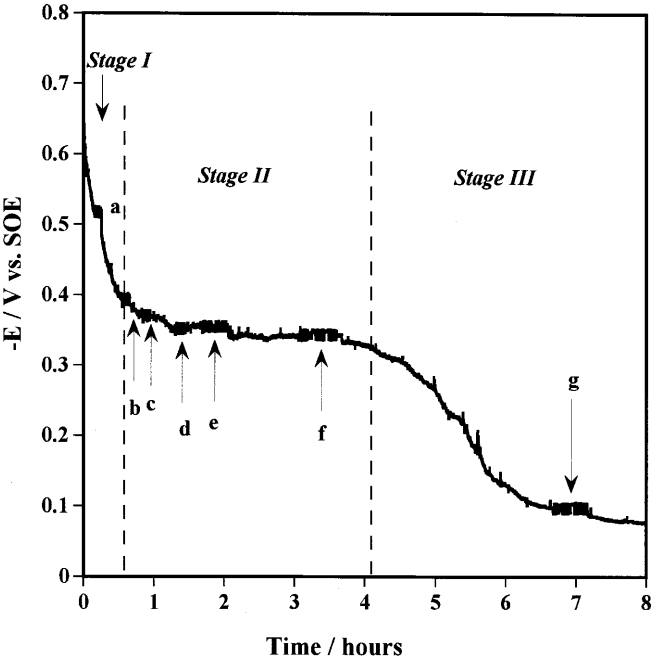

Fig. 1 Open circuit potential (OCP) of a nickel electrode immersed in a Li_2CO_3-K_2CO_3 (62–38 mol%) eutectic melt at 650 °C under an oxidizing atmosphere of O_2/CO_2 (90/10) at a total pressure of 1 atm. Sample thickness is 0.75 μm

around –0.74 V vs. SOE, then gradually decreased to reach a potential around –0.34 V vs. SOE (referred as to stage II), where it stayed at this value for about 3.5 h. Finally, after another decrease, the electrode potential approached the oxygen reduction equilibrium potential (referred as to stage III).

Figure 2 illustrates AFM surface scan images of the surface samples withdrawn from the melt at the different stages shown on the OCP curve. It is clearly seen that a compact surface Ni oxide is formed during stage I of the nickel oxidation (Fig. 2a). This surface is atomically flat. At stage II of the OCP curve, the oxide layer became thicker (Fig. 2b). Large grains and small grains are both evident on this surface. The structure within each grain is also clearly measured, having the same growth direction. On the 3D images, one can see a few hillocks formed which outcrop above the surface. The islands, some of which have begun to merge, indicate that growth by three-dimensional nucleation can proceed. After 2 h of exposure, agglomerates in a rounded mass are formed (Fig. 2c). We have to point out that no grain boundary grooving has been observed for all the surfaces scanned.

In addition to imaging surfaces, the AFM can also be used to determine surface roughness [12]. Figure 3 shows the evolution of the surface roughness root mean square (r.m.s.) of the nickel electrode upon exposure time in the Li + K carbonate melt. As can be seen, the surface of the nickel electrode has roughened. However, we have to emphasize that the r.m.s. measurements reported here were carried out on a size scale of 20×20 μm and do not represent the whole area of our samples (0.39 cm^2). Roughness measurements made by AFM often depend on the size scale over which the roughness is measured. For example, one could imagine a surface that is quite rough (or smooth), but one could image only one small area with the AFM that might look quite smooth (or rough) on that size scale. In practice, the values of the surface roughness r.m.s. depend on the measuring instrument. The length of the sample, the area resolution, and the sampling rate all affect the parameter. A confocal laser scanning microscope or an optical interferometric device can both provide detailed surface information, including roughness, over a much larger scanned region than can an AFM (but with much lower resolution than an AFM).

Figure 4 shows the evolution of XRD patterns of the nickel electrode during the different stages reported in Fig. 1. It can be seen that the reaction mechanism is complicated and a sequential series of reactions occurs. The observed Bragg peak positions (Table 1) agree well with those reported in the reference patterns for Ni (JCPDS no. 4-850), NiO (JCPDS no. 78-0423), $NiCO_3$ (JCPDS no. 12-771), and Au (JCPDS no. 4-784). Two salient features of the XRD results are observed:

1. The appearance of the $NiCO_3$ compound. This compound appeared in the beginning of the oxidation process (i.e., after 1 min upon exposure) and then vanished after 2 h of exposure. Formation of an unstable but unidentified compound during the oxidation of Ni in molten carbonates has been also postulated on the basis of in situ XRD studies [13].
2. Detailed examination of the XRD data revealed that the (200) Bragg peak for NiO slightly shifted toward lower angles from 30 min of exposure (corresponding to point b in Fig. 1). The lattice parameter (unit cell) has also increased, which indicates that the NiO lattice has expanded. This is ascribed to lithium incorporation into the NiO lattice. No highly lithiated nickel oxide has been detected by XRD. This is because the amount of lithium incorporated into the

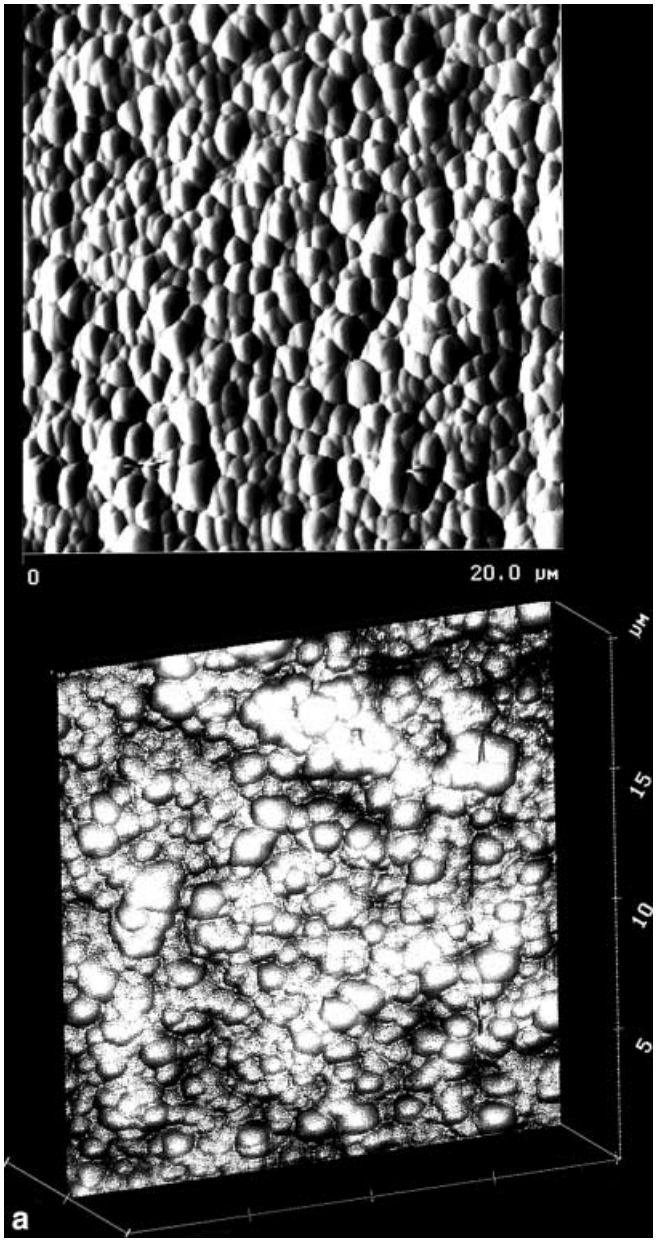

Fig. 2 AFM images of nickel samples withdrawn from the melt at the different stages shown in Fig. 1: **a** stage I, $t = 1$ min; **b** stage II, $t = 35$ min; **c** stage II, $t = 2$ h

Fig. 2 (Contd.)

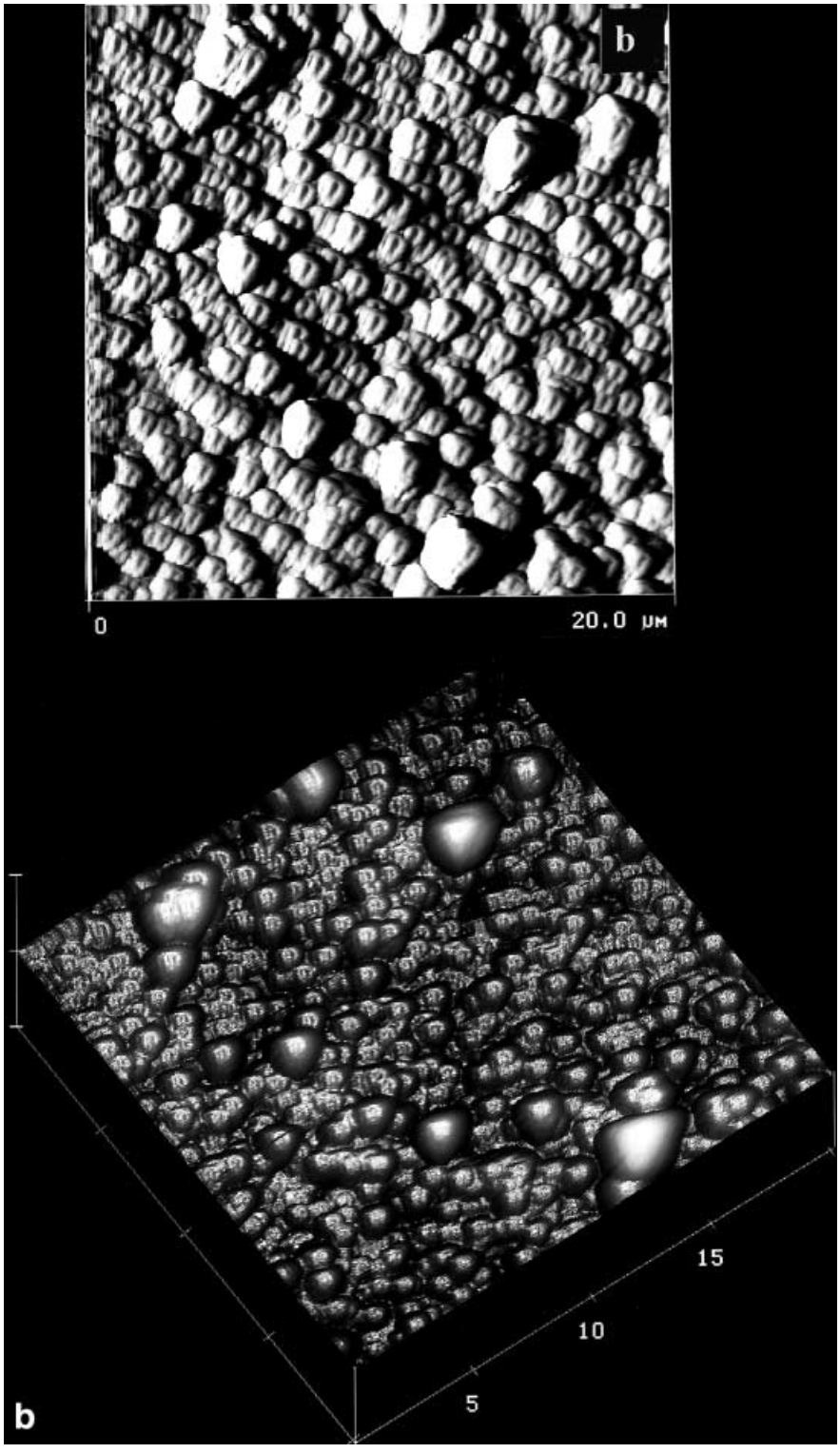

NiO matrices is very low and therefore the X-ray diffraction is not sensitive enough with respect to the low concentration of lithium in NiO.

We employed EDS for qualitative analysis of those elements present in the sample, with regard to the amount of each. For that purpose, we used well-characterized standard reference materials. For nickel probing, we employed a nickel polycrystalline plaque, whereas for lithium and oxygen we used spodumene ($LiAlSi_2O_6$). The amount of carbon was automatically deduced. The ZAF (atomic number, absorption, and fluorescence) matrix correction routines have been carried out for the matrices of both unknown and the

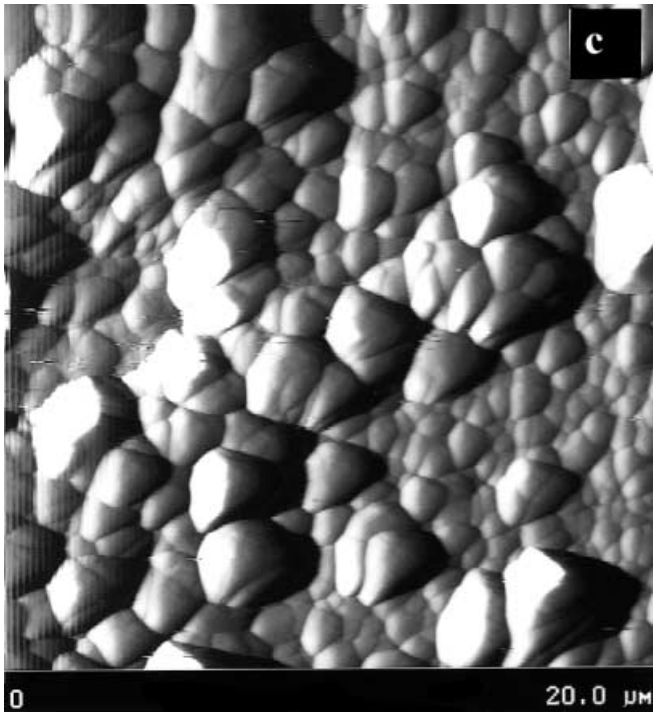

Fig. 2 (Contd.)

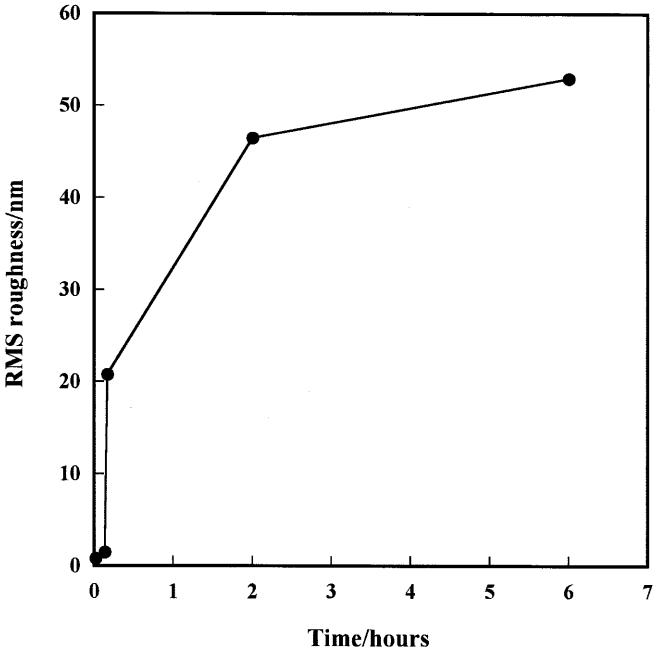

Fig. 3 Evolution of the nickel surface roughness r.m.s. with exposure time in the Li_2CO_3-K_2CO_3 (62–38 mol%) eutectic melt

interference standard [14]. Depending on the sample areas, EDS showed that in addition to nickel (80–91 mol%) and oxygen (5–25 mol%), up to 2–33 mol% of carbon was present. With regard to the lithium content, more refined techniques than EDS are required. Some researchers have observed the presence of lithium by Fourier transform infrared spectroscopy (FTIR) [15]. Others have estimated the lithium content at about 1–4 atom% [16]. However, these observations were qualitative or semi-quantitative. Application of more sophisticated techniques for the quantitative determination of the lithium content in NiO has been done recently by Belhomme et al. [17] The authors employed the nuclear microprobe technique and found that the lithium amount varies between 0.1 and 0.5 atom%, depending on the melt exposure duration and the analyzed position in the layer thickness. The authors argued that the atmosphere considered in their work was probably not rich enough in oxygen ($air + CO_2 = 70 + 30$) to yield the formation of highly lithiated nickel oxide, namely $LiNiO_2$. However, an oxygen-rich atmosphere was used in our experimental conditions ($O_2 + CO_2 = 90 + 10$) and no such lithiated nickel oxide was revealed.

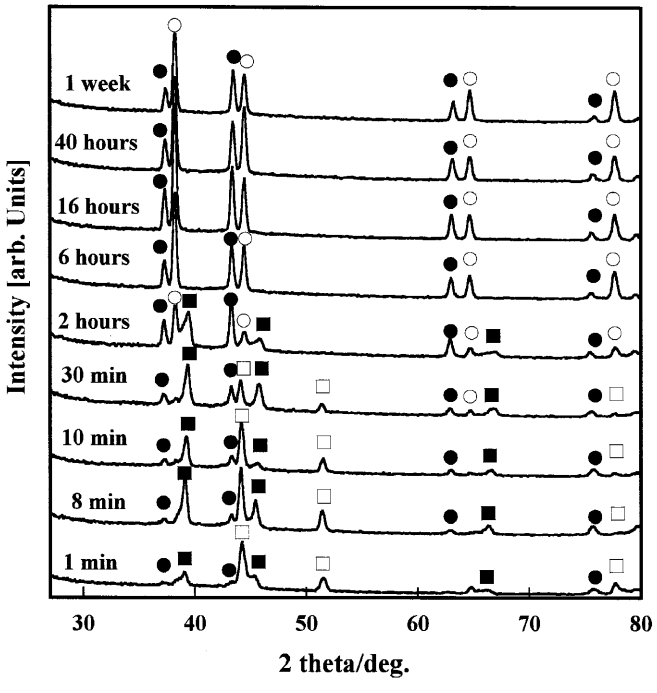

Fig. 4 XRD data of nickel samples withdrawn from the melt at various times of exposure: Au (○), Ni (□), NiO (●), $NiCO_3$ (■)

EIS measurements

Complex impedance spectra recorded at each point marked with characters on the OCP curve shown in Fig. 1 are illustrated in Fig. 5. A system which consists of a metal covered by an oxide film is often quite complex and may involve a large number of different situations. Our particular interest lies in the information that can be learned from a.c. impedance measurements; it is necessary to apply a simple model (equivalent circuit) to present the following results in a meaningful and representative way.

Table 1 XRD identification of the various elements involved during the oxidation of nickel in Li_2CO_3-K_2CO_3 (62–38 mol%) at 650°C under O_2/CO_2 (90/10) gas atmosphere. The subscript ref refers to JCPDS data

	h	*k*	*l*	d_{obs} (Å)	d_{ref} (Å)	$\lvert\Delta d\rvert/d_{obs}$
NiO	1	1	1	2.4137	2.4127	0.0004
	2	0	0	2.0904	2.0895	0.0004
	2	2	0	1.4775	1.4775	0.0000
	3	1	1	1.2597	1.2600	0.0002
	2	2	2	1.2064	1.2063	0.0001
$NiCO_3$	1	1	0	2.3090	2.3040	0.0021
	1	1	3	2.0890	2.0860	0.0014
	2	1	4	1.4010	1.3960	0.0035
Ni	1	1	1	2.0380	2.0340	0.0019
	2	0	0	1.7730	1.7620	0.0062
Au	1	1	1	2.3510	2.3550	0.0017
	2	0	0	2.0386	2.0390	0.0002
	2	2	0	1.4400	1.4420	0.0013
	3	1	1	1.2297	1.2300	0.0002

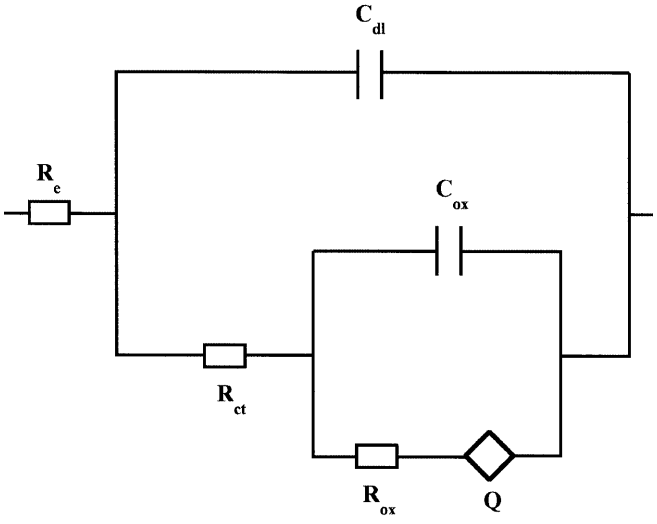

Fig. 5 The Nyquist (**a**) and Bode plots (**b**) for the nickel electrode recorded at the points shown in Fig. 1: **a** (●), **b** (○), **c** (■), **d** (□), **e** (✦), **f** (✧), and **g** (+)

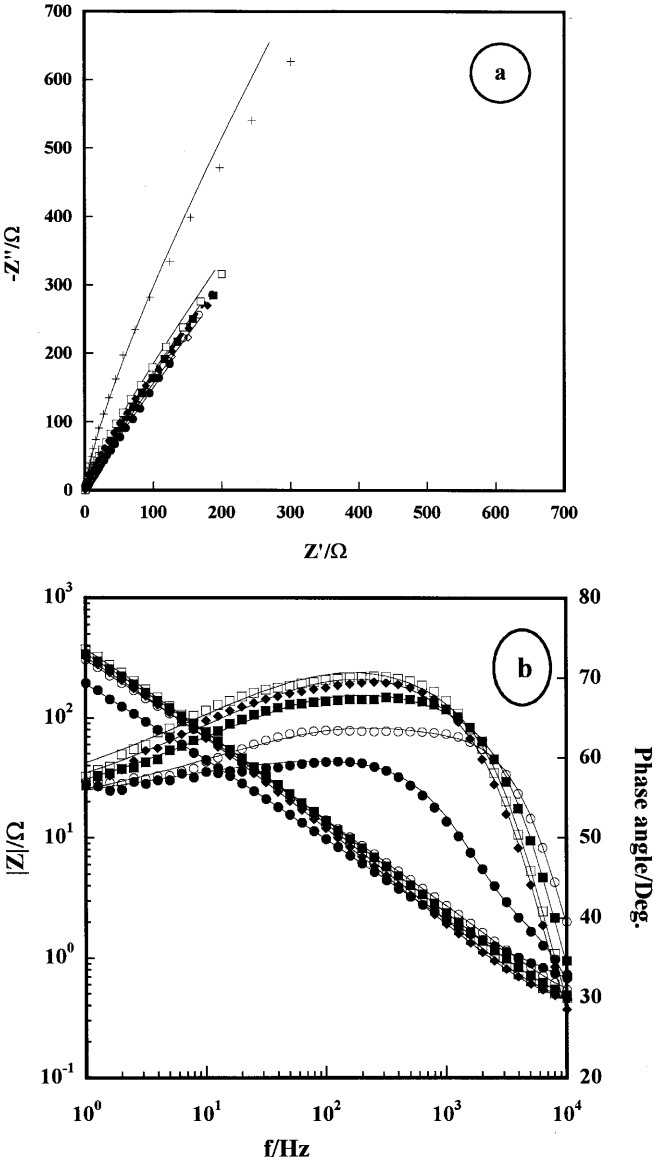

Fig. 6a, b Equivalent circuit used to fit impedance spectra shown in Fig. 5

The equivalent circuit that was found to describe satisfactorily the observed impedance spectra is depicted in Fig. 6. The fitted data agree well with the measured data. The Re component in the circuit is the electrolyte resistance. The R_{ct}, C_{dl} parallel network stands for the electrochemical behavior of the oxide/melt interface and thus represents the charge transfer resistance and the double layer capacitance, respectively. The second R_{ox}, C_{ox} parallel network is originated by the presence of the electrical barrier properties in the oxide layer, so it describes the resistance and the capacitance of the bulk phase of the oxide layer, respectively. The sum of R_{ct} and R_{ox} may also be defined as $R_s = R_{ct} + R_{ox}$. Parameters of interest deduced from the fitting procedure are listed in Table 2. In this table are also reported χ^2 and the average estimated error, δ, in the residual plots. The exponent of the constant phase element Q has a value for n lower than 0.6, which means that it is close to the Warburg diffusion element. The Warburg response observed during stage I (point a in Fig. 1) is due to the formation of the oxide layer (or corrosion of Ni metal) on the electrode surface, which exhibits a shielding effect on mass transport of the reactants such as metal ion or metal vacancy. The Warburg coefficient, σ^{-1}, has a small value. Hence, the reciprocal value is large, which means that the diffusion of metal ions through the oxide scale is probably the slowest reaction step. The value of σ^{-1} decreases upon exposure time (the reciprocal value increases), which indicates that the diffusion proceeds slower. This is probably due to the contribution of Li^+ ion diffusion in the compact oxide layer. After point d, the Warburg coefficient assumes a constant value. The double layer capacitance, C_{dl}, increases as the exposure

Table 2 Fit results of impedance spectra recorded during the oxidation of a nickel electrode immersed in Li_2CO_3-K_2CO_3 (62–38 mol%) at 650 °C under an O_2/CO_2 (90/10) gas atmosphere

	R_e (Ω)	$R_s = R_1 + R_2$ (Ω)	C_{dl} (μF)	σ^{-1} ($s^{0.5}/\Omega$)	n	χ^2	δ (%)
a	0.47	4.84	38.4	1.6×10^{-3}	0.59	1.1×10^{-4}	3
b	0.39	5.48	44.6	1.0×10^{-3}	0.58	7.0×10^{-5}	2
c	0.39	7.80	56.3	8.7×10^{-4}	0.57	1.1×10^{-4}	3
d	0.39	9.27	67.9	7.5×10^{-4}	0.58	7.3×10^{-5}	2
e	0.39	7.99	73.3	9.1×10^{-4}	0.57	6.4×10^{-5}	2
f	0.39	5.63	80.0	1.1×10^{-3}	0.58	5.4×10^{-5}	2
g	0.39	4.75	394.4	1.0×10^{-3}	0.59	2.0×10^{-4}	5

time increases and is in agreement with the formation of a porous oxide layer. The R_s value of the nickel electrode increases owing to the formation of a poorly conducting oxide layer at its surface; after reaching a maximum, it decreases asymptotically.

The impedance diagram recorded at point g has been discarded in the present paper. It is clear from Fig. 5 that the equivalent circuit of Fig. 6 no longer satisfactorily describes the electrode response. At that stage, the electrode is highly porous and reaches the oxygen electrode reaction under these gas conditions. The equivalent circuit in Fig. 6 must be refined. This will be the topic in a separate paper.

Discussion

Putting together all the results obtained by means of AFM, XRD, EDS, and by a.c. impedance, the following simplified reactions can be assigned to the different stages observed from the OCP curve, which was plotted according to immersion time:

1. The first stage clearly corresponds to the oxidation of nickel to nickel oxide. The oxidation of nickel can proceed through the formation of an intermediate unstable compound, namely $NiCO_3$, according to the following sequences of electrochemical and chemical reactions as stipulated by Tomczyk et al. [3]:

$$Ni + CO_3^{2-} \rightarrow NiCO_3 + 2e \quad (3)$$

$$NiCO_3 \rightarrow NiO + CO_2 \quad (4)$$

   This oxide layer is formed quickly (1 min upon exposure), accompanying CO_2 evolution. This oxide layer is compact, poorly conducting, and causes limitations on the further transport of oxygen to the Ni/NiO phase boundary.
2. The second stage reflects the oxide growth and lithiation process. It has been reported that pure nickel oxide can be near stoichiometric, but this compound tends to be a cation-defective p-type nickel oxide [18]. This means that nickel vacancies are the major defects. Therefore, at the second stage, divalent nickel ions are expected to be present in the lattice. The oxidation of some of these divalent nickel ions to trivalent nickel ions within the oxide scale may proceed according to the following electrochemical reaction, given in the defect chemical notation of Kröger and Vink [19]:

$$2Ni_{Ni} + O^2 \rightarrow 2Ni'_{Ni} + V''_{Ni} + O_o + 2e \quad (5)$$

   where the oxide is supplied by the dissociation of the carbonate ions.
   The formation of trivalent nickel ions is accompanied by the incorporation of Li^+ in the nickel oxide lattice, which can be described by the following chemical reaction:

$$V''_{Ni} + 2Li^+ + O^2 \rightarrow 2Li'Ni + O_o \quad (6)$$

   Before lithiation takes place, the oxide layer decreases the effective conductivity of the nickel electrode. After the resistance reaches a maximum as seen in Table 2, it decreases to the order of magnitude of semiconductor resistance. The presence of lithium in the lattice increases the concentration of trivalent nickel ions in the nickel oxide lattice because of the occupied vacancies, as discussed by Yazici and Selman [5]. The lithiation reaction is thus evident from the reduction of the R_s value as the reaction progresses from the beginning to the end of stage II. Reactions similar to Eqs. 5 and 6 have been also postulated by Vossen et al. [20].
3. In the third stage, the NiO electrode reaches the oxygen equilibrium potential, and behaves as a conductive oxide whose potential corresponds to the oxygen reduction equilibrium. This stage requires the electrode to be fully oxidized and lithiated, thereby forming a porous structure.

Conclusion

Nickel oxidation in a molten Li_2CO_3-K_2CO_3 melt has been characterized by means of the OCP response, AFM, XRD, EDS, and by a.c. impedance. The combination of these techniques allowed further the provision of relevant information on the oxidation of nickel. AFM, used for the first time, provided conclusive evidence that nickel oxidation passes through the rapid formation of a compact surface oxide (stage I), a thicker oxide layer (stage II), and a porous oxide structure (stage III). XRD and EDS both permitted identifying the different compounds formed during the different stages of the nickel oxidation. Importantly, the nickel carbonate compound has been identified and the amount of carbon has been evaluated. The lithiation reaction has been identified as occurring during the second stage of the nickel oxidation. This process was recognized by means of XRD and impedance analysis.

Acknowledgements This work was supported by the Proposal-Based Immediate-Effect R&D Promotion Program no. 98Z31-011 from the New Energy and Industrial Technology Development Organization (NEDO).

References

1. Nishina T, Takizawa K, Uchida I (1989) J Electroanal Chem 263:87
2. Tomczyk P, Mordarski G, Oblakowski J (1993) J Electroanal Chem 353:177
3. Tomczyk P, Sato H, Yamada K, Nishina T, Uchida I (1995) J Electroanal Chem 391:125
4. Young Yang B, Young Kim K (1998) Electrochim Acta 43:3343
5. Yazici MS, Selman JR (1999) Solid State Ionics 124:149
6. Liu C-T, Devereux OF (1991) J Electrochem Soc 138:386
7. Vossen JPT, Ament PCH, de Wit JHW (1996) J Electrochem Soc 143:2272
8. Uchida I, Nishina T, Mugikura Y, Itaya K (1986) J Electroanal Chem 206:229
9. Uchida I, Mugikura Y, Nishina T, Itaya K (1986) J Electroanal Chem 206:241
10. Uchida I, Nishina T, Mugikura Y, Itaya K (1986) J Electroanal Chem 209:125
11. Boukamp BA (1989) Equivalent circuit user's manual. University of Twente, Netherlands
12. Hues SM, Colton RJ, Meyer E, Guntherodt HJ (1993) MRS Bull 18:41
13. Xie G, Sakamura Y, Ema K, Ito Y (1990) J Power Sources 32:125
14. Scott VD, Love G, Reed SJB (1995) Quantitative electron-probe microanalysis. Ellis Horwood, Chichester, UK
15. Malinowska B, Cassir M, Devynck J (1996) J Power Sources 63:27
16. Selman JR, Marianowski LG (1982) In: Lovering DG (ed) Molten salt technology. Plenum Press, New York, p 323
17. Belhomme C, Cassir M, Tessier C, Berthoumieux E (2000) Electrochem Solid State Lett 3:216
18. Koide S, Takei H (1963) J Phys Soc Jpn 18:319
19. Kröger FA, Vink HJ (1956) Solid State Phys 3:307
20. Vossen JPT, Plomp L, de Wit JHW (1994) J Electrochem Soc 141:3041